# Polarization Mode Control of Two-Dimensional Photonic Crystal Laser by Unit Cell Structure Design

Susumu Noda,[1,3]* Mitsuru Yokoyama,[2,3] Masahiro Imada,[1,3] Alongkarn Chutinan,[1,3] Masamitsu Mochizuki[1,3]

We demonstrate polarization mode selection in a two-dimensional (2D) photonic crystal laser by controlling the geometry of the unit cell structure. As the band diagram of the square-lattice photonic crystal is influenced by the unit cell structure, calculations reveal that changing the structure from a circular to an elliptical geometry should result in a strong modification of the electromagnetic field distributions at the band edges. Such a structural modification is expected to provide a mechanism for controlling the polarization modes of the emitted light. A square-lattice photonic crystal with the elliptical unit cell structure has been fabricated and integrated with a gain media. The observed coherent 2D lasing action with a single wavelength and controlled polarization is in good agreement with the predicted behavior.

Photonic crystals (PCs) have drawn much attention as a new type of optical material with a periodic refractive index, where a photonic bandgap that has the ability to selectively block optical wavelengths is formed (*1*–*6*). Various scientific and engineering applications are expected to be developed using the photonic bandgap and artificially introduced defects and/or light-emitters. Recent progress toward developing photonic crystal technology includes single defect-mode lasing in a 2D photonic bandgap structure (*7*) and 2D coherent lasing based on multidirectionally distributed feedback effect in a 2D PC structure (*8*, *9*). The latter device operates with current injection (*8*), and applications such as large-area 2D surface-emitting lasers with stable single longitudinal and lateral modes are expected. Such stable control of the electromagnetic field distribution across a large area is a notable feature of PC-based devices and cannot be achieved by other types of lasers such as vertical cavity surface-emitting lasers (VCSELs) (*10*) or circular grating coupled surface-emitting lasers (CGSELs) (*11*). This ability to control originates from the unique properties of the 2D photonic lattice (*8*, *12*).

However, an issue that remains regarding the 2D photonic crystal laser is the complex polarization mode of the emitted light. Even though the individual longitudinal and lateral modes are single, the polarization mode control has not yet been achieved. Control of the polarization mode is expected to give rise to lasers with desirable features such as perfect single-mode emission over a large area, high-output power, and surface emission with a very narrow divergence angle. In this study, we show that the polarization mode can be controlled by deforming the unit cell structures in 2D PCs with a square lattice.

A schematic of the structure of the 2D photonic crystal with a square lattice and a circular-shaped unit cell is shown in Fig. 1A. The crystal has two specific directions, Γ-X and Γ-M. In the dispersion relation, or the band diagram, of the structure (Fig. 1B), it is expected that lasing occurs at specific points on the Brillouin zone boundary and at points of band crossing and splitting when optical gain is supplied. At these points, or band edges, waves propagating in different directions couple, and a standing wave is formed. For example, if we consider the point S in Fig. 1B, light with wavelength equal to the period of the Γ-X direction is important (white arrow in Fig. 1A). When the light propagates in an arbitrary Γ-X direction (0°), it is diffracted not only to the backward Γ-X direction (180°) but also to the perpendicular Γ-X directions (±90°) because the Bragg conditions are also satisfied. The 2D diffraction induces the coupling of light waves propagating in all four Γ-X directions, resulting in the formation of a 2D standing wave in the PC plane. The point S is particularly interesting in that it gives the in-plane coupling of four Γ-X directions to form the lasing cavity, and light is simultaneously diffracted in the direction perpendicular to the PC surface because the Bragg condition is also satisfied in that direction. Thus, coherent 2D large-area surface-emission with stable longitudinal and lateral modes can be achieved.

From the detailed band structure at the point S (Fig. 2A), one can see that there are four band edges (I, II, III, and IV) arising from the in-plane coupling of light waves propagating in the four Γ-X directions. One pair (III, IV) is doubly degenerate and the other (I, II) are nondegenerate. The electromagnetic field distributions in the PC plane for individual edges according to the plane-wave expansion method (Fig. 2, B and C) correspond to the nondegenerate band edges I and II. The amplitudes of magnetic fields in the direction perpendicular to the plane are indicated by red and blue areas, representing positive and negative, respectively. The arrows show the electric field vectors in the plane, and the thick black circles indicate the locations of lattice points. The individual electric field distributions are complicated, resulting in complicated polarization. The electromagnetic field distribution at band-edges III and IV cannot be determined concretely due to the degeneracy and, thus, cannot be shown in a figure. The field distribution is considered to be determined by an environmental or operational condition and as such is very unstable. Therefore, polarization mode control using the circular structure will be difficult.

The situation changes markedly when we deform the unit cell structure from the circular to the elliptical shape (Fig. 3A). The electromagnetic field distributions at individual band edges are shown in Fig. 3, B through E, for the introduction of the elliptical unit cell to individual lattice points, where the elliptical ratio (the ratio of short- to long-axes) is 0.7. The degeneracy of band edges III and IV (Fig. 2A) is completely resolved, and the energy separation between I and II becomes large. (Here, we denote the new band edges as I′, II′, III′, and IV′.) More important, the electric field distributions at individual band edges become unified or linear (Fig. 3, B through E). As a result, very simple linear polarization can be expected for any of these band edges. The asymmetric structure of the ellipse not only resolves the degeneracy of band edges, but also induces the alignment of the electric magnetic field in one direction. This fact can be understood also by the group theory. The frequencies of individual modes are determined according to the amount of electric field distribution in the region of the elliptical unit cell with a lower refractive index than the surrounding region, which yields a frequency separation between individual band edges. It was also found that

[1]Department of Electronic Science and Engineering, Kyoto University, Yoshida-honmachi, Sakyo-ku, Kyoto 606-8501, Japan. [2]Research and Development Headquarters, Minolta, Ltd., 1-2 Sakura-machi, Takatsuki, Osaka 569-8503, Japan. [3]Core Research for Evolutional Science and Technology (CREST), Japan Science and Technology Corporation (JST), Kyoto 606-8501, Japan.

*To whom correspondence should be addressed. E-mail: snoda@kuee.kyoto-u.ac.jp

the frequency separation can be controlled by changing the elliptical ratio of individual unit cells. Previously, we used a 2D PC with triangular lattice (*8*, *12*). We have found that the effect of deforming the unit cell structure of a square lattice for polarization control is much more effective than using a triangular lattice. The details of this difference will be reported elsewhere (*13*).

Encouraged by these promising theoretical results, we fabricated a 2D PC laser by integrating the PC with a gain media by the wafer-fusion technique (Fig. 4A). The 2D PC structure is formed on an n-InP substrate (wafer B). The gain media is formed in wafer A by sandwiching an InGaAsP/InP multiple-quantum-well active layer with an emission wavelength of 1.3 μm between p-InP and thin n-InP cladding layers. Both wafers were stacked and heated in a hydrogen atmosphere at 620°C and were bonded firmly. The inset of Fig. 4A is a scanning electron microscopy (SEM) image of the elliptical unit cells formed in wafer B with a lattice constant of 400 nm. A 300-μm-diameter gold electrode was evaporated on the surface of the bonded wafer. Therefore, the electrode does not cover the entire area of the square lattice, allowing the surface-emitted light to be observed from the surrounding area. The light output–current characteristic is shown in Fig. 4B, revealing that lasing has been successfully achieved at room temperature. The near-field pattern of lasing and the spectra and polarizations at representative positions were measured (*14*). Despite the large diameter of the device,

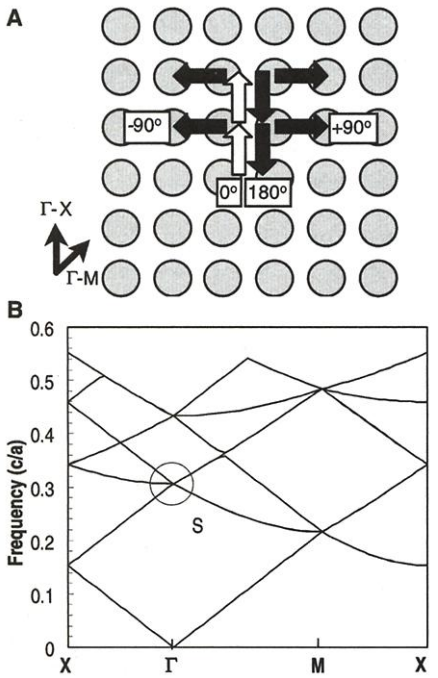


**Fig. 1.** (**A**) Schematic of 2D photonic crystal structure with square lattice and circular unit cell. The two specific directions Γ-X and Γ-M are indicated. In-plane diffraction related to the point S in (**B**) is also shown. (**B**) Dispersion relation or band diagram of structure for transverse-electric (TE)–like mode, calculated by plane-wave expansion method with dielectric constants of unit cell and surrounding material of 10.56 and 10.92, respectively. The area fraction occupied by the unit cell was assumed to be 0.2.

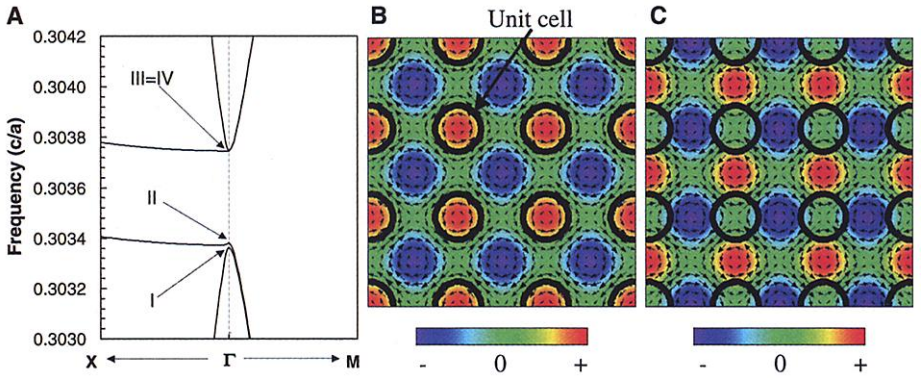


**Fig. 2.** (**A**) Detailed band structure of point S in Fig. 1B. (**B** and **C**) Electromagnetic field distributions at band edges I and II, respectively. Amplitudes of magnetic fields in the direction perpendicular to the plane are indicated by red and blue areas (positive and negative). Arrows indicate the electric field vectors in the plane, and thick black circles indicate the locations of lattice points.

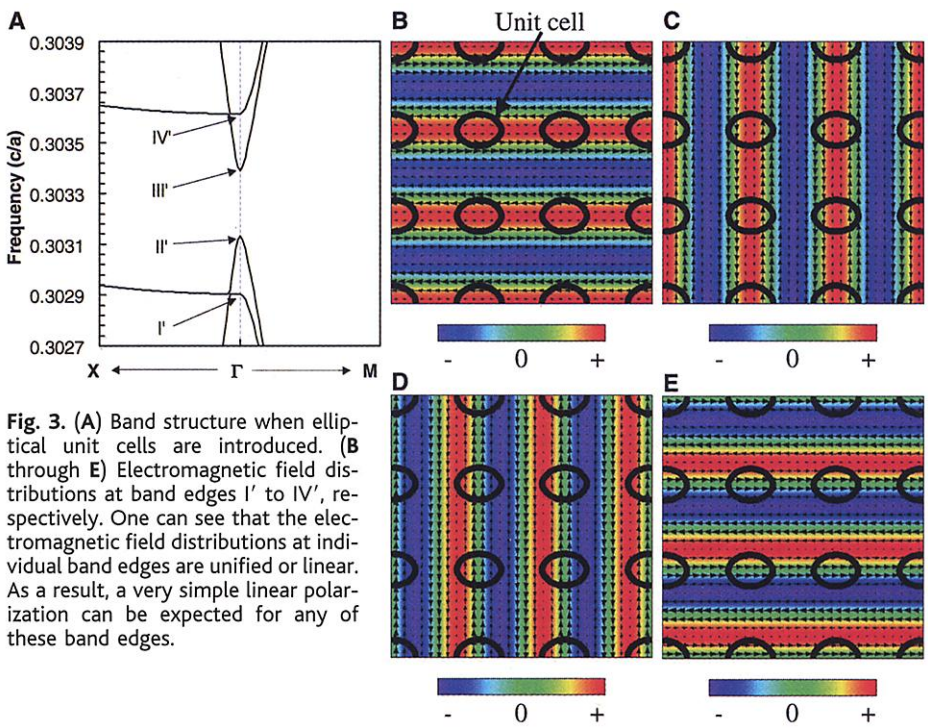


**Fig. 3.** (**A**) Band structure when elliptical unit cells are introduced. (**B** through **E**) Electromagnetic field distributions at band edges I′ to IV′, respectively. One can see that the electromagnetic field distributions at individual band edges are unified or linear. As a result, a very simple linear polarization can be expected for any of these band edges.

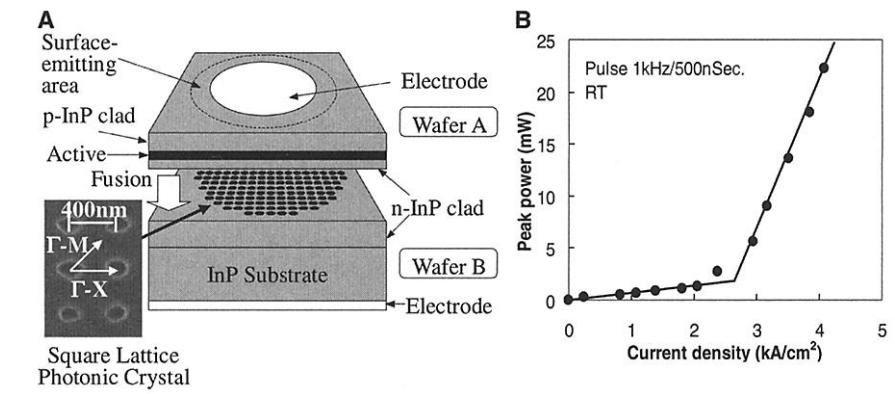


**Fig. 4.** (**A**) Schematic of 2D photonic crystal laser structure with square lattice and elliptical unit cells fabricated in this study. (**B**) Light output–current characteristic of device at room temperature.

single wavelength and linear polarization have been successfully achieved. In the case of the other lasers (VCSEL or CGSEL), when the area of the laser cavity becomes very large, the lateral mode becomes multimode because no mechanism for lateral mode control is present, leading to multimodal lasing in terms of wavelength and polarization. Also, the near-field pattern extends to the long-axis direction of individual elliptical unit cells. The lasing is considered to occur at either band edge II′ or III′ (Fig. 3) when we compare the obtained near-field pattern and the polarization with the results shown in Fig. 3, B through E. As the Poynting vector is directed toward the long axis of elliptical unit cells in band edge II′ or III′, the near-field pattern spread in only one direction. All the measured elliptical devices lased in the same manner. In separately fabricated 2D PCs with circular unit cells, the observed near-field patterns extended in two perpendicular directions, rendering control of the polarization mode very difficult. On the basis of these results, the deformation of the unit cell structure in 2D PC lattice constitutes an effective means of controlling the polarization mode of PC surface emission.

**References and Notes**


1. E. Yablonovitch, *J. Opt. Soc. Am. B* **10**, 283 (1993).
2. S. John, *Phys. Today* **44**, 32 (1991).
3. N. Vats, S. John, *Phys. Rev. A* **58**, 4168 (1998).
4. J. D. Joannopoulos, P. R. Villeneuve, S. Fan, *Nature* **386**, 143 (1997).
5. S. Noda, K. Tomoda, N. Yamamoto, A. Chutinan, *Science* **289**, 604 (2000).
6. S. Noda, M. Imada, A. Chutinan, *Nature* **407**, 608 (2000).
7. O. Painter *et al.*, *Science* **284**, 1819 (1999).
8. M. Imada *et al.*, *Appl. Phys. Lett.* **75**, 316 (1999).
9. M. Meyer *et al.*, *Appl. Phys. Lett.* **74**, 7 (1999).
10. For example, S. Uchiyama, K. Iga, *IEEE J. Quantum Electron.* **QE-22**, 301 (1986).
11. For example, C. M. Wu *et al.*, *IEEE Photon. Tech. Lett.* **4**, 960 (1992).
12. M. Imada, A. Chutinan, S. Noda, M. Mochizuki, *Phys. Rev. B*, in preparation.
13. M. Yokoyama, S. Noda, unpublished data.
14. Web figure 1 is available at *Science* Online at www.sciencemag.org/cgi/content/full/293/5532/1123/DC1.



15. Supported in part by a grant-in-aid for scientific research of priority areas from the Ministry of Education, Culture, Sports, Science, and Technology of Japan; Kyoto University VBL; and ICF Foundation.

19 April 2001; accepted 5 July 2001


# High-Temperature Ferromagnetism in $CaB_2C_2$


**J. Akimitsu,[1,2]* K. Takenawa,[1] K. Suzuki,[3] H. Harima,[4] Y. Kuramoto[5]**



**We report a high Curie–temperature ferromagnet, $CaB_2C_2$. Although the compound has neither transition metal nor rare earth ions, the ferromagnetic transition temperature $T_c$ is about 770 Kelvin. Despite this high $T_c$, the magnitude of the ordered moment at room temperatures is on the order of $10^{-4}$ Bohr magneton per formula unit. These properties are rather similar to those of doped divalent hexaborides, such as $Ca_{1-x}La_xB_6$. The calculated electronic states also show similarity near the Fermi level between $CaB_2C_2$ and divalent hexaborides. However, there is an important difference: $CaB_2C_2$ crystallizes in a tetragonal structure, and there are no equivalent pockets in the energy bands for electrons and holes—in contrast with $CaB_6$. Thus, the disputed threefold degeneracy, specific to the cubic structure, in the energy bands of divalent hexaborides turns out not to be essential for high-temperature ferromagnetism. It is the peculiar molecular orbitals near the Fermi level that appear to be crucial to the high-$T_c$ ferromagnetism.**


The search for magnets with high ferromagnetic transition temperatures ($T_c$'s) is not only of practical interest but is also of basic scientific interest, in identifying the mechanism. The origin of the high-$T_c$ ferromagnetism observed in doped hexaborides was initially attributed to electron correlations in the low-density electron gas (*1*), and much attention has been paid to the band structure of the divalent hexaborides (*2*, *3*). It has been postulated that the presence of three equivalent valleys in the energy bands plays an important role in the formation of excitonic ferromagnetism (*4*–*6*). However, the fact that this has been observed only in this particular class of compounds has caused difficulty in identifying the mechanism of this phenomenon. This study reveals that the high-$T_c$ ferromagnetism is not a singular phenomenon but that a similar ferromagnetism appears in a tetragonal compound, $CaB_2C_2$, without the band degeneracy. Our observation may provide a route for preparation of new high-$T_c$ ferromagnets.

Powder samples of $CaB_2C_2$ were prepared from Ca shot (99%), amorphous powder boron (99%), and powder carbons (99%). The starting materials were mixed at the stoichiometric ratio Ca:B:C = 1: 2:2 in an argon glovebox, pressed into pellets, and placed in a wrapped tantalum tube. The pellets were then heated in two ways: (i) at 1050°C for 20 hours in 2000 atm of an argon atmosphere in a hot isostatic-pressing furnace, and (ii) at 1050°C for 30 hours in a vacuum quartz tube. In both cases, reddish-brown powders of $CaB_2C_2$ were obtained. Because the samples are sensitive to moisture, they were handled under an argon atmosphere.

In the x-ray diffraction patterns obtained (Fig. 1), most of the diffraction peaks can be indexed to the tetragonal structure, consistent with an earlier structural study (*7*) of $CaB_2C_2$. There are slight amounts of impurity phases of CaO and $CaB_6$ in the sample, as seen in the corresponding weak intensity. The inset of Fig. 1 shows the two-dimensional network formed by boron (B) and carbon (C) atoms in $CaB_2C_2$. The Ca ions sit on each vertex and center of the square and sandwich each B-C layer. Depending on the stacking of B-C layers along the *c* axis, the crystal symmetry becomes either simple tetragonal (*P*4/*mbm*) lattices or body-centered tetragonal (*I*4/*mcm*) lattices. The latter has the sequence B-C-B-C- . . . along the *c* axis, whereas the former has B-B- . . . (and C-C- . . .) stacking. Experimentally, these two different structures can be distinguished only by observing a signal corresponding to the B-C superstructure along the *c* axis. Unfortunately, the x-ray scattering intensity is too weak to identify or disprove such a signal. Hence, the crystal structure of $CaB_2C_2$ has not yet been experimentally fixed. On the other hand, it has been established that related compounds $RB_2C_2$ with trivalent rare earth ion R have *P*4/*mbm* (*8*, *9*).

Magnetization measurements with a SQUID magnetometer (Fig. 2, inset) show the magnetization versus applied magnetic fields at $T = 5$ K. The diamagnetic contribution of the sample holder was independently measured by removing the sample, and this background has been subtracted. The magnetization shows a characteristic feature of ferromagnetism, with the saturation moment of $3.8 \times 10^{-4}$ Bohr magneton ($\mu_B$) per formula unit [or 2.1 electromagnetic units (emu) per mole of formula] at 1 T, which is comparable


[1]Department of Physics, Aoyama-Gakuin University, Tokyo 157–8572, Japan. [2]Core Research for Evolutional Science and Technology (CREST) of the Japan Science and Technology Corporation, Japan. [3]Faculty of Environmental and Information Sciences, Yokohama National University, Yokohama 240–8501, Japan. [4]Institute of Scientific and Industrial Research, Osaka University, Osaka 567-0047, Japan. [5]Department of Physics, Tohoku University, Sendai 980-8578, Japan.

*To whom correspondence should be addressed. E-mail: jun@phys.aoyama.ac.jp